Ionics (2023) 29:3437–3450
https://doi.org/10.1007/s11581-023-05087-8

REVIEW

Conducting behaviour of a novel solid biopolymer electrolyte for electrochemical application

S. Rehila Karolin Blesstina[1] · T. Mathavan[1] · P. Buvaneshwari[1] · T. Joel[1] · A. Milton Franklin Benial[1]

Received: 23 January 2023 / Revised: 1 June 2023 / Accepted: 10 June 2023 / Published online: 20 July 2023

Abstract

A novel optimised solid biopolymer electrolyte (SBE) was fabricated based on flaxseed gum (FG) with various concentration of ammonium chloride (NH_4Cl) via solution casting technique. The characterizations of the SBE film were made using X-ray diffraction (XRD), Fourier transform infrared (FTIR), differential scanning calorimetry (DSC), scanning electron microscopy (SEM) and electrochemical impedance spectroscopy (EIS). The XRD pattern reveals significant enhancement of amorphous nature with incorporation of NH_4Cl. The existence of interaction between FG and NH_4Cl was proven through FTIR. DSC predicts the glass transition temperature T_g to be 52.34 °C. On addition of 0.3 M wt% NH_4Cl, the EIS showed increase in ionic conductivity from 2.95×10^{-9} S/cm (pristine FG) to 1.13×10^{-4} S/cm. The conductivity trend was further verified by dielectric analysis, which proved the non-Debye behaviour. Using the highest conducting SBE film, the open circuit voltage was found to be 1.89 V at 353 K.

Keywords Ionic conductivity · Flaxseed gum · Ammonium chloride · Biopolymer electrolyte · Impedance study · Dielectric behaviour

Introduction

The increasing demand for high-performance electrochemical devices such as batteries [1, 2], supercapacitors [3], fuel cells [4] and photochemical solar cells [5] with good flexibility, high energy and power density and environmentally benign, have brought an enormous interest towards identifying new bio-friendly materials. An electrolyte is an essential component in the application of electrochemical devices, acting as a bridge to promote free-moving ions from anode to cathode and vice versa [6]. It can be in the form of solid, liquid or gel materials with the ability to conduct ions but not the electrons. Portable electronic devices such as laptops, tablets, mobile phones and power banks have batteries that contain liquid electrolyte [7]. The leakage is the common problem with the liquid electrolyte between the electrodes with significant drawbacks. So, attention has been required in the development of SBE. In SBEs, the host materials can be synthetic polymers such as polyvinyl alcohol [8], polyethylene oxide [9] and polyvinyl chloride or natural polymers. The use of synthetic polymers in electrochemical devices can be replaced by alternative biobased polymers, as a solution to environmental degradation [10]. Hence, SBE can be used as an electrolyte in batteries to efficiently transport ions between the electrodes (cathode and anode) while being as thin as possible. An ideal electrolyte should be achieved high bulk ionic conductivity beyond 10^{-4} S/cm at ambient temperature and should act as an electronic insulator by which ion transport can be facilitated and possess minimum amount of self-discharge. In general, ionic conductivity is proportional to the number of mobile ions, the mobility of the charge carriers and temperature. The number of mobile ions depends on the degree of dissociation of dopant in the polymer matrix. So as to improve the ionic conductivity, distinct organic or inorganic salts were incorporated into biopolymers that provide ions for conduction.

Immense effort has been devoted in exploring superior polymers in nature. Based on natural polymer, a number of polysaccharide electrolytes have been fabricated from a variety of natural resources like carrageenan [11, 12], agar–agar [13], gellan gum [14, 15], cellulose acetate [16] and chitosan [17]. Monisha et al. have reported 50 cellulose acetate: 50

✉ T. Mathavan
tjmathavan@gmail.com

[1] PG & Research Department of Physics, N.M.S.S Vellaichamy Nadar College (Affiliated to Madurai Kamaraj University), Nagamalai, Madurai 625019, Tamil Nadu, India

NH_4SCN has the maximum conductivity of 3.31×10^{-3} S/cm. The findings confirms that the increase in conductivity is due to increase in NH_4SCN concentration [1]. Meera Naachiyar et al. found that 1 g Gellan gum with 1.1 M wt% of NH_4SCN exhibits highest conductivity of 1.41×10^{-2} S/cm with very high amorphous nature and OCV of 1.62 V [14]. Selvalakshmi et al. synthesised agar–agar doped with NH_4Cl and obtained maximum ionic conductivity of 4×10^{-3} S/cm at room temperature which exhibits Arrhenius behaviour [13]. Among various natural polymer host, cellulose-based materials have been attracted significant attention towards electrochemical energy storage devices. The flaxseed mucilage is a biopolymer, substantially present in the outermost layer of the seedcoat. Flaxseed gum (FG) is an anionic polysaccharide with abundant hydroxyl (–OH) and functional group that provide many coordination sites for cation. It is mainly composed of 75% neutral arabinoxylans (D-galactose, D-xylose, L-arabinose) and 25% acidic rhamnogalacturonan (L-rhamnose, L-fucose, L-galactose and D-galacturonic acid) which provide good rheological, mechanical strength and film-forming property [18–23]. Safdar et al. reported the average molecular weight of flaxseed gum is 1.32×10^6 (1322 kDa) [20]. Figure 1 shows the structure of FG. The mucilage from flaxseeds has high water-binding capacity which correlates to high affinity between solvent and separator with higher conductivity [22]. So far, FGs are widely used in the treatment of numerous diseases as well in food, cosmetic, agricultural and pharmaceutical application. The present study is the first to ever document FG as a biopolymer electrolyte for electrochemical application.

Inorganic salts provide transportation of charge carriers in the polymer matrix by Grotthuss conducting mechanism. In proton-conducting biopolymer system, ammonium salts are substantial proton donors to the polymer matrix. Correspondingly, the cationic (NH_4^+) and anionic (Cl^-) radii for NH_4Cl were found to be 151 pm and 167 pm, respectively, with lattice energy of 674.02 kJ/mol [9]. Lattice energy is responsible for the dissociation of ions as cation and anion. The lower the lattice energy, the facile the dissociation of ions. The lattice energy of NH_4Cl is slightly higher compared to other ammonium salts. Here, H^+ ion of NH_4^+ cations is the conducting species in FG-NH_4Cl system. One of the hydrogen atom of NH_4^+ ions is weakly bound and it can easily dissociate under the influence of electric field. Thus, the effect of electric field migrates the hydrogen ion (H^+) from one coordination site to another along the polymer chain or hops from one chain to another. In solid-state electrolytes, the ionic conductivity is a vital factor for futuristic battery application. As a result, the highest conducting FG-NH_4Cl system had shown a promising performance and has a great potential to be applied in proton based energy device application for example in proton batteries. The aim of this work focuses on developing a novel solid proton conducting biopolymer electrolyte from flaxseed mucilage doped with NH_4Cl.

Materials and methods

Materials

Flaxseed (*Linum uistatissimum* L.) grains were purchased commercially and washed thoroughly using demineralized water. Ammonium chloride (molecular weight = 53.49 g/

Fig. 1 Structure of FG

mol) was purchased in analytical grade from Isochem Laboratories, Kochi. Demineralized water is used to extract FG. All materials were used without any purification.

Methods

Extraction of FG

The FG was extracted by hot water extraction method, besides FG with NH_4Cl-based polymer electrolytes were prepared by solution casting technique. Figure 2 shows the schematic diagram of the preparation of the film. The flaxseeds (30 g) were mixed and soaked in 300 ml of demineralized water in a ratio of 1:10. To produce an optimal mucilage solution, the soaked flaxseeds were stirred at 400 rpm for 1 h using hotplate magnetic stirrer at boiling temperature [20, 24]. The results of heat exposure to flaxseed actually resulted in etching effect on seed coat and release of gum polysaccharides [25]. To acquire the mucilage solution, the mixture was then filtered and cooled to room temperature.

Membrane preparation

Different concentrations of NH_4Cl (0.1 to 0.4 wt%) was added to 30 ml of mucilage solution. Table 1 shows the designation of FG-NH_4Cl films. The solutions were magnetically stirred continuously at 300 rpm for 24 h at ambient temperature for complete dissolution. The solutions were cast in petri dishes and dried in a hot air oven at 60 °C until thin films were formed. These obtained free standing films were of thickness ranging from 40–100 µm.

Characterization of the membrane

Detailed characterisation of the biopolymer electrolyte was undertaken. XRD patterns were recorded using XPERT-PRO diffractometer Cu-Kα radiation operated with 40 kV/30 mA at 2θ angles between 10° and 80°. The degree of crystallinity (X_c) of the polymer electrolyte was calculated using the deconvolution technique. Fourier-transform infrared spectra (FTIR) were performed with IRAFFINITY-1 CE Shimadzu spectrometer to study the complexation between FG and NH_4Cl in the polymer electrolyte. The infrared radiation through the film beams at frequency ranging from 400 to 4000 cm^{-1} at room temperature. The impedance, dielectric and ionic conductivity of the polymer electrolytes were determined by AC impedance technique using HIOKI-3532 LCR HiTester system over a wide range of frequency from 42 Hz to 5 MHz. Direct current (DC) polarisation technique was used to measure transference number and transient ionic current. The transference numbers t_+ and t_- were determined using Wagner's DC polarisation technique with the DT830D SEW multimeter by sandwiching the highest conducting polymer electrolyte between two stainless steel electrodes with a fixed dc voltage of 1.5 V. DSC measurements were recorded using DSC Q20 V24.11 build 124 instrument under nitrogen atmosphere in the temperature

Table 1 Composition of flaxseed gum-NH_4Cl

Sample designation	Flaxseed gum (ml)	NH_4Cl (M wt%)
FG0	30	0
FG01	30	0.1
FG02	30	0.2
FG03	30	0.3
FG04	30	0.4

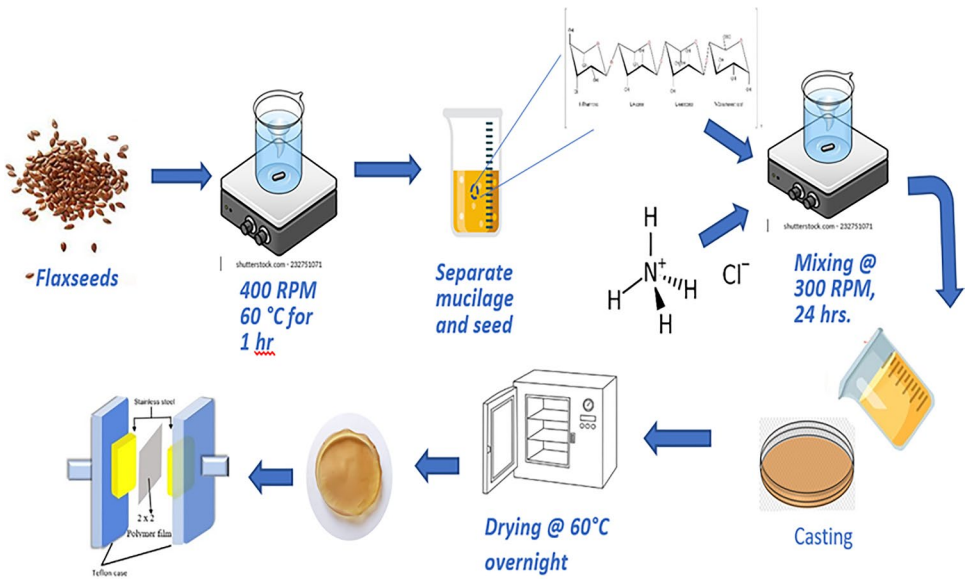

Fig. 2 Schematic diagram of preparation of film

ranging from 20 to 150 °C. The morphology of the SBE films was monitored using VEGA3 TESCAN microscope with an accelerating voltage of 20 kV. Dielectric properties and electric modulus studies of the polymer electrolyte give the electrode polarisation effects of FG-NH_4Cl films.

Battery fabrication

A proton battery was fabricated using the highest conducting membrane as an electrolyte. A mixture of zinc metal powder, zinc sulphate and graphite were grinded together and pressed into pellets and used as an anode electrode. Similarly, the cathode material comprises lead dioxide (PbO_2), vanadium pentoxide (V_2O_5), graphite powder and the highest conducting polymer electrolyte [14]. The highest conducting film was sandwiched between anode and cathode and assembled in a sample holder and the OCV measurement were carried out with DT830D SEW multimeter.

Results and discussion

XRD analysis

The observed diffraction patterns of the prepared FG polymer electrolytes are shown in Fig. 3. However, most findings suggest that the amorphous phase with activated chain segments easily supports ion transportation. The question of whether amorphous or crystal nature can transport ions faster is still controversial [26]. Therefore, it is thought that one of the best strategies to increase ionic conductivity is to increase amorphous phase of the polymer electrolyte. Rashid et al. found pure FG has a broad diffraction peak at 2θ = 20° which indicates a lack of crystallinity [19]. In the pure FG pattern Fig. 3a, a broad hump centred at 20° is attributed to amorphous structure of the FG polymer chain. This corresponds to the irregular brunching polysaccharide structure and due to the electrostatic repulsion between the anionic chains [27]. This broad amorphous hump in the FG spectra broadens with an increase in the concentration of NH_4Cl, which has been due to the interaction of the polymer and the salt. On addition of NH_4Cl, few sharp peaks appeared at 2θ = 22.8°, 32.5°, 40.1°, 47.02°, 52.8° and 58.2° with their orientations being (100), (110), (111), (200), (210) and (211) respectively, which originated from crystalline nature of pure NH_4Cl (JCPDS card no. 34–0710). We could notice a peak at 27.8° (JCPDS card no. 01–084-0799), which might be due to the chloride ion, particularly when NH_4Cl is dissolved in water; it yields NH_4^+ and Cl^- ions. The addition of NH_4Cl into the FG matrix showed a remarkable increase in the intensity of peaks. The presence of sharp peaks in Fig. 3(e) confirms that the polymer can no longer solvate the salt. Therefore, a substantial amount of salt has been deposited on the surface of the film. This eventually decreases the number of mobile ions which in turn decreases the conductivity of the film as evident from the Nyquist plot. Salleh et al. reported the similar trend of XRD pattern on addition of ionic dopant [28].

The crystalline and amorphous peaks are perceived using deconvolution method by Origin software. Figure 3(B) shows the deconvoluted XRD patterns of the polymer

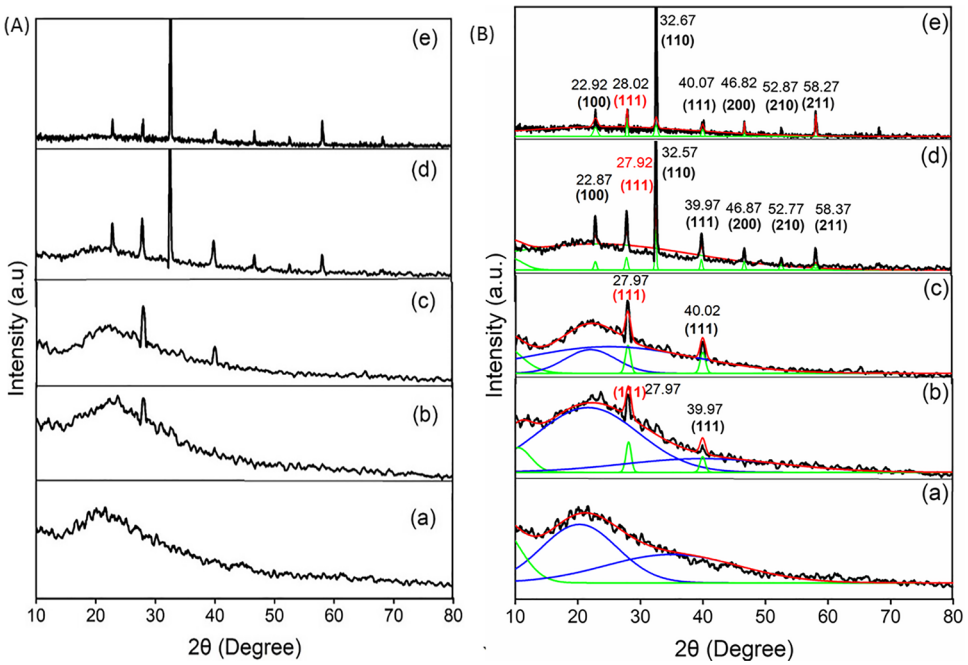

Fig. 3 XRD pattern and deconvoluted XRD pattern of the biopolymer electrolyte (A) XRD pattern of (a) FG0, (b) FG01, (c) FG02, (d) FG03, (e) FG04. (B) Deconvoluted XRD pattern of (a) FG0, (b) FG01, (c) FG02, (d) FG03, (e) FG04

electrolytes. The degree of crystallinity (X_c) has been calculated from the equation below:

$$X_c(\%) = \frac{A_c}{A_c + A_a} \times 100 \quad (1)$$

where Ac and Aa are the area under crystalline and amorphous region, respectively. From Table 2, it is obvious that the degree of crystallinity decreases with addition of salt causing reduction in the energy barrier. The reduction in crystallinity enhances the conductance of the polymer electrolyte. Hodge et al. reported the relation between the peak intensity and degree of crystallinity [29].

FTIR analysis

The FTIR analysis is an effective technique to identify the functional group present and is used to track the complex formation between salt and polymer matrix. Figure 4 depicts FTIR spectra of FG-NH_4Cl system. It has been observed that changes in peaks at 3282 cm^{-1}, 2919 cm^{-1}, 1627 cm^{-1}, 1433 cm^{-1}, 1075 cm^{-1}, 807 cm^{-1} and 638 cm^{-1} is due to addition of NH_4Cl upon FG matrix. From Fig. 4(a), the strong and broad band at 3282 cm^{-1} region is the result of stretching vibration of abundant hydroxyl groups (OH). The shift in wavenumber of this hydroxyl group was due to the complex formation between polymer matrix and NH_4Cl. The band at 2919 cm^{-1} is responsible for CH stretching of CH_2 group in cellulose [30]. It can be seen that this band disappeared upon the incorporation of NH_4Cl. This indicates that there is a strong interaction between the polymer matrix and the ionic dopant.

Figure 4(b) shows two peaks responsible for C = O and C–OH stretching. The absorption at 1627 cm^{-1} was attributed to C = O asymmetric stretching vibration of carboxyl group (COOH) in galacturonic acids in the FG matrix which acts as a binding site for ions [18, 25]. Under the influence of an electric field, the weekly bound H^+ of NH_4^+ can be easily dissociated and hops through the C = O coordinating site of the FG matrix. It can be seen that the C = O stretching of COO^- of the polymer matrix is shifted towards lower wavenumbers, i.e. from 1627 to 1604 cm^{-1} upon addition of NH_4Cl. This may be due to the weakening of C = O bond due to

Table 2 Degree of crystallinity of FG complexes

Sample	Degree of crystallinity (%)
FG0	24.78
FG01	23.26
FG02	12.01
FG03	9.48
FG04	5.42

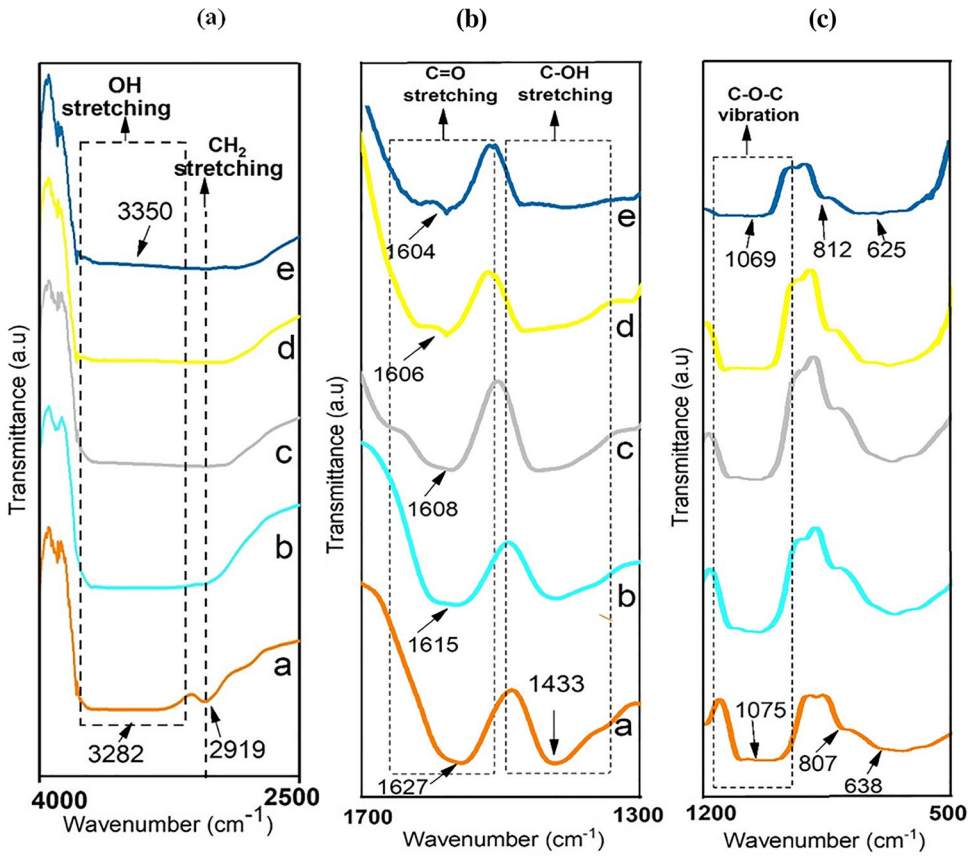

Fig. 4 FTIR spectra of the biopolymer electrolyte (a) FG0, (b) FG01, (c) FG02, (d) FG03, (e) FG04

Table 3 FTIR peak assignments for pure FG0 and highest conducting electrolyte FG03

Wave numbers (cm^{-1})		Peak assignments	References
FG0	FG03		
3282	3350	OH stretching vibration	46
2919	–	CH stretching CH_2 of cellulose	31, 32, 47, 50
1627	1604	C = O stretching vibration of galacturonic acid	31, 32, 50
1433	1482	C–OH symmetric stretching	31, 46
1075	1069	C–O–C pyranose ring vibration	46
807	849	Presence of α-D-galactose	32, 46
638	641	Polymer backbone bending	31

Table 4 FTIR mode of C = O band vibrations in FG complexes

Sample	C = O band vibration Wavenumber (cm^{-1})	Force constant k (N/cm)
FG0	1627	1.068
FG01	1615	1.053
FG02	1608	1.043
FG03	1606	1.041
FG04	1604	1.038

removal of electron density. More H^+ ions were delivered into the polymer matrix with the addition of NH_4Cl, increasing the interaction with COO^- [31]. Thus, H^+ ions interacted with FG polar group (COO^-) when NH_4Cl is added into the biopolymer. The shifting of C = O to lower frequency was occurred possibly due to decreased force constant of C = O bond (Table 4). As the concentration increases, the C = O stretching mode begins to split with a shoulder at 1780 cm^{-1}. This splitting indicates that the C = O group formed a hydrogen bond with the OH group and shifted towards lower frequency [32]. The absorption band at 1433 cm^{-1} is ascribed to symmetric stretching vibration of C=O or C–OH and existence of uronic acid [20, 27]. The intensity of the peak decreases and begins to disappear.

Another noticeable complexation based on Fig. 4(c) is the broad band at 1075 cm^{-1}, which indicates stretching of C–O–C pyranose ring [21, 27]. A slight shift in wavenumber from 1075 to 1069 cm^{-1} and decrease in intensity were observed. The band at 807 cm^{-1} refers to the presence of α-D-galactose and the peak at 638 cm^{-1} may be due to the bending of the polymer backbone [20]. The various shifts in peaks and their vibrations are listed in Table 3. It is evident that as the concentration of salt increases, the number of H^+ ions also increases in the polymer system, which leads to the shift in the band intensities and vibrations.

The C = O vibrational band shows significant shift in frequency of the FTIR spectra. The relation between shift in frequency and force constant can be determined from Eq. (2) [33, 34].

$$\bar{\nu} = \frac{1}{2\pi c}\sqrt{\frac{k}{\mu}} \tag{2}$$

where $\bar{\upsilon}$ is the wavenumber (cm^{-1}), c is the velocity of light (3×10^{10} cm/s), k is the force constant (N/cm) and μ is the reduced mass of two atoms is given by Eq. (3).

$$\mu = \frac{M_1 M_2}{M_1 + M_2} \tag{3}$$

where M_1 and M_2 are the atomic weights of two atom, respectively. The force constant of C = O stretching for the biopolymer electrolytes is calculated and tabulated in Table 4. We could notice that the force constant value decreases from 1.068 to 1.038 N/cm as the concentration of salt increases. This is due to the interaction of H^+ ions in NH_4Cl with the COOH in the polymer matrix. This confirms the complex formation between host polymer and salt.

SEM analysis

A scanning electron microscope (SEM) was employed to investigate the morphology of the film surface. SEM micrographs were recorded for both the pristine sample and the highest conducting polymer film FG03. Figure 5 shows the observed SEM images of FG0 and FG03 electrolytes. Microscopic views of FG0 (Fig. 5a) showed uniform surface morphology with some breaks, which is due to the scratches on the surface of the petri dish formed during film-synthesis process. On the other hand, the micrographs of the highest conducting film (Fig. 5b) shows an interesting morphology with some particulates and ion aggregates, which indicates that NH_4Cl particles are randomly dispersed on the surface. Further increasing the concentration leads to formation of NH_4Cl particles as clusters and a dopant-rich surface (crystalline). Further agglomeration of NH_4Cl particles does not contribute to ionic conduction, which forms intense crystalline peaks that support the outcomes of XRD.

DSC analysis

Differential scanning calorimetry was carried out to investigate the thermal behaviour of the polymer electrolyte. Figure 6 shows the glass transition temperature T_g of the prepared samples. The temperature at which the polymer material changes from a rigid glassy state to a soft rubbery state is called glass transition temperature T_g [35]. The

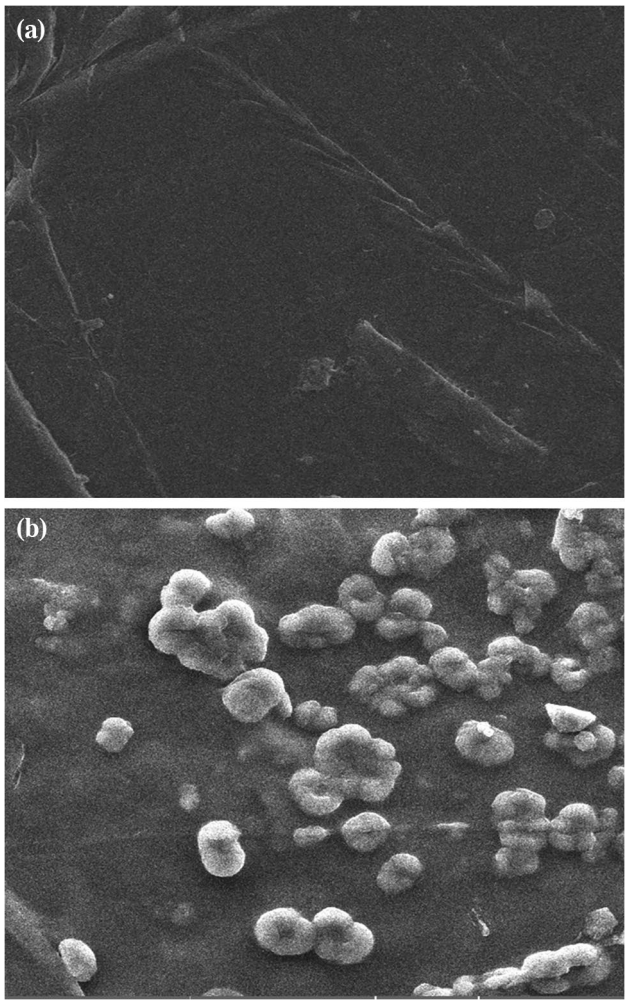

Fig. 5 SEM images of (**a**) FG0 and (**b**) FG03

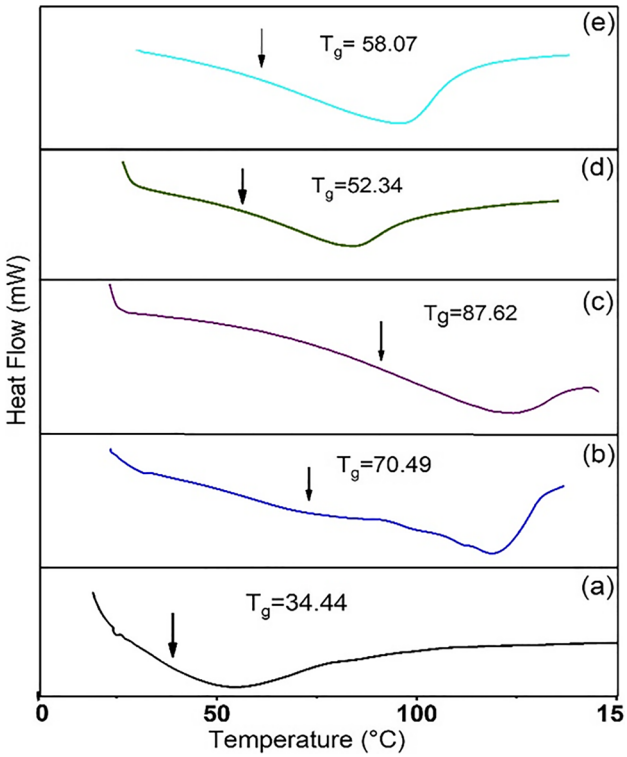

Fig. 6 DSC thermograms of the biopolymer electrolyte **a** FG0, **b** FG01, **c** FG02, **d** FG03, **e** FG04

Table 5 Glass transition temperatures of FG-NH_4Cl polymer electrolytes

Sample	Glass transition temperature T_g (°C)
FG0	34.44
FG01	70.49
FG02	87.62
FG03	52.34
FG04	58.07

thermogram exhibits a single-step transition of an endothermic process that confirms the complexation of host polymer and dopant. The midpoint of transition is measured as T_g in which there could be higher ion mobilisation. The T_g of pristine FG was 34.44 °C. The lowest value for FG0 indicates that the polymer electrolyte is highly amorphous that is analogous with the XRD results. The T_g value shifts towards the higher temperature side, due to incorporation of NH_4Cl. The T_g of the prepared polymer electrolytes is tabulated in Table 5. There is an increase in T_g from 34.44 to 58.07 °C which is due to increase in stiffness of host polymer with addition of NH_4Cl that impedes ionic transport. It is observed that there is a decrease in T_g value for FG03. In general, the decrease in T_g increases the ionic conductivity owing to high segmental motion of the polymer electrolyte. This segmental motion produces space that easily transports ions. Again the increase in T_g for FG04 is due to undissociated salt in the polymer matrix which is also confirmed from XRD result [36]. Buvaneshwari et al. reported the similar behaviour of T_g with increasing salt concentration [26].

EIS analysis

Electrochemical impedance measurement is an effective, non-destructive technique used to determine the electrical characteristics of polymer electrolyte materials. The impedance plot of the polymer electrolyte films at ambient temperature (303 K) are shown in Fig. 7. The impedance is a complex number of real and imaginary part linked with resistive and capacitive process respectively. The Nyquist plot contains a semi-circle at the high-frequency region and a tail in the low-frequency region. The diameter of the depressed semicircle gives the charge transfer resistance, and the linear part reflects the constant phase element and

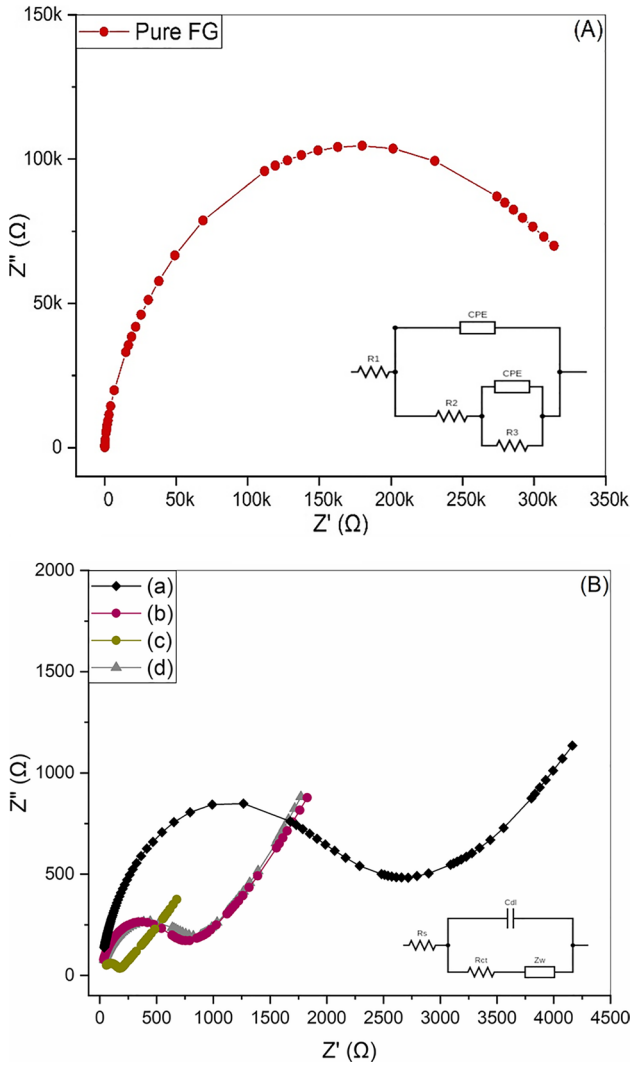

Fig. 7 The Nyquist plot of the biopolymer electrolyte at room temperature with its electrical equivalent RC circuit. (A) Nyquist plot of pure flaxseed film with its equivalent circuit. (B) Nyquist plot of (a) FG0, (b) FG01, (c) FG02, (d) FG03, (e) FG04 with its equivalent circuit

Warburg resistance (W) and diffusion process [34]. The interaction between the semi-circle and real axis gives the bulk resistance (R_b). The conductivity of the polymer electrolytes can be calculated using Eq. (4)

$$\sigma = \frac{t}{R_b \times A} Scm^{-1} \quad (4)$$

Here, t is the thickness of the film, R_b is the bulk resistance (from the Nyquist plot) and A is the electrode–electrolyte contact area (cm^2). Table 6 shows the R_b and ionic conductivity of the SBE system. The increasing ionic conductivity with increasing concentrations of NH_4Cl is due to enormous number of mobile charge carriers. The

Table 6 Resistance and Conductance of FG-NH_4Cl SBE system

Compositions	*Bulk resistance* R_b *(Ω)*	*Ionic conductivity* σ *(S/cm)*
FG0	2.95245×10^5	2.95×10^{-9}
FG01	2.794×10^3	6.91×10^{-6}
FG02	7.90×10^2	2.68×10^{-5}
FG03	$\boldsymbol{1.88} \times 10^2$	$\boldsymbol{1.13} \times 10^{-4}$
FG04	8.88×10^2	2.39×10^{-4}

conductivity of pure FG electrolyte FG0 has been found to be 2.95×10^{-9} S/cm and the highest ionic conductivity is 1.13×10^{-4} S/cm for FG03. Anandha et al. obtained highest conducting polymer electrolyte of 1.53×10^{-6} S/cm for 25 wt% NH_4Cl added to SPBEs [37]. Shreedatta et al. reported a maximum conductivity of 1.81×10^{-3} S/cm for 7.5 wt% NH_4Cl/PVA [38]. The NH_4Cl dopant introduced free ammonium cation (NH_4^+) and chloride (Cl^-) anion to be dissociated. The NH_4^+ cations have an ideal tetrahedral structure of three tightly bound hydrogen atom and one weekly bound hydrogen atom which can easily dissociate. This poorly bound H^+ ion in NH_4^+ can hop from one site to its neighbouring site (interacts with the functional group) leaving a vacancy [13]. This vacancy will be occupied by other H^+ ion in the polymer matrix. This exchange of proton between FG-NH_4Cl complexed sites is responsible for the conduction mechanism. This transport of protons declares the Grotthus mechanism. It is obvious that the ionic conductivity decreases with the addition of NH_4Cl above 0.4 wt% which is ascribed to neutral aggregation of ions re-association or formation of ion clusters that blocks the conduction routes for ion transport [39]. The equivalent circuit's network was fitted using ZsimpWin software which evaluates the processes inside the polymer electrolyte in order to study its electrochemical behaviour. Figure 7(A, B) show an electrical equivalent circuit (Randles model), which is a modelling of electrochemical double layer that fits the EIS data. The circuit comprises parameters R_{ct}, C_{dl} and Z_w representing charge transfer resistance, capacitance due to electrochemical double layer and Warburg impedance due to ion diffusion respectively, in the electrolyte. From the Nyquist plot it is seen that the R_{ct} for FG-NH_4Cl systems is smaller than the pristine FG0, demonstrating that FG-NH_4Cl system has highest charge transfer rate compared to the undoped system.

Dielectric behaviour

The study of dielectric properties is a tool for obtaining information about the conductive behaviour and ionic molecular interactions of the polymer electrolyte. The dielectric response of free moving charge carriers is usually

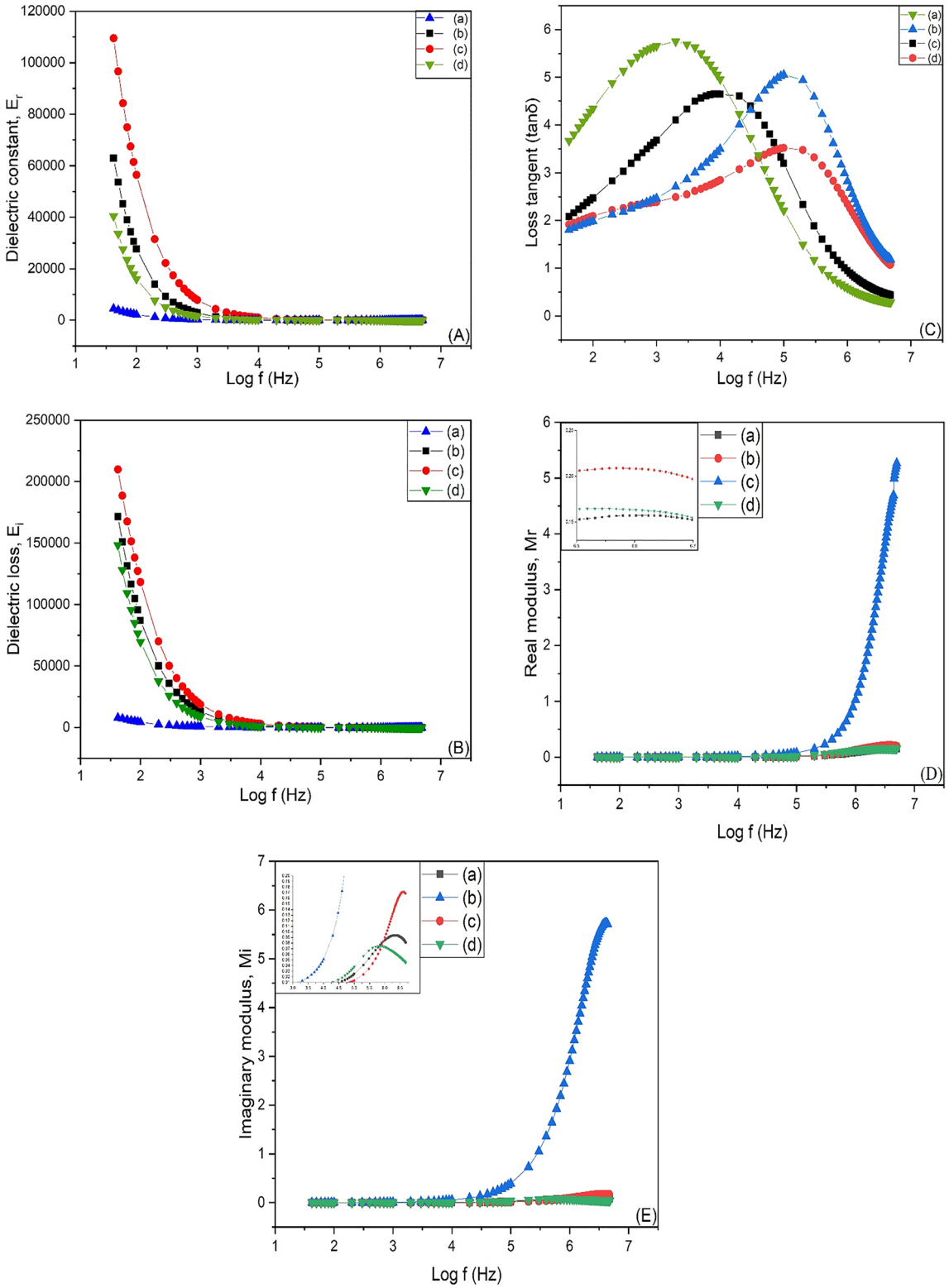

Fig. 8 Frequency dependence of the biopolymer electrolyte (A) Frequency dependence of ε_r of (a) FG01, (b) FG02, (c) FG03, (d) FG04. (B) Frequency dependence of ε_i of (a) FG01, (b) FG02, (c) FG03, (d) FG04. (C) Frequency dependence of tangent loss (tan δ) of (a) FG01, (b) FG02, (c) FG03, (d) FG04. (D) Frequency dependence of M_r (a) FG01, (b) FG02, (c) FG03, (d) FG04. (E) Frequency dependence of $M_i$of (a) FG01, (b) FG02, (c) FG03, (d) FG04

dominated by the diffusion coefficient [36]. Figure 8 shows the dielectric plots for the polymer electrolytes at ambient temperature. The real and imaginary part of complex permittivity is given by Eq. (5).

$$\varepsilon^* = \varepsilon' - i\varepsilon'' = \varepsilon' - i\left(\sigma'/\omega\varepsilon_0\right) \tag{5}$$

Here, ε′ real part of the dielectric constant, ε″ imaginary part of dielectric constant, σ′ real part of conductivity, ω angular frequency and ε_0 permittivity of free space.

The dielectric constant is the measure of ability to store energy in the form of charge (acts as a capacitor in electric field) and the dielectric loss is the material's dissipation factor, which describes how incident energy is lost inside the material in an electric field and how it gets dissipated inside the material. In most cases, the diffusion coefficient dominates the dielectric response of free mobile charge carriers and not due to molecular dynamics. The process of diffusive charging is called electrode polarisation which creates the electrochemical double layer. Figure 8(A, B) shows variations in permittivity ε′ and ε″ as a function of frequency for the FG-NH_4Cl polymer electrolytes. The dielectric constant ε′ and dielectric loss ε″ is high at lower frequencies which indicates the increase in dielectric polarisation, and as frequency increases, they fall off that shows a declination of polarisation due to charge accumulation. ε′ and ε″ of the highest conducting FG03 film have a high value of 109 K at 42 Hz and gradually drop until frequency 5 K Hz, and beyond this frequency it remain constant which confirms the non-Debye behaviour. The electric dipoles have ample time to align with the applied field, before they change direction at low frequencies. Since the dipoles at higher frequencies do not have sufficient time to align themselves with the direction of the applied field, due to accumulation of charges, both ε′ and ε″ values are low. The dielectric loss of FG03 exhibited a relaxation peak at low-frequency region. The relaxation peak at low frequency means longer relaxation time. The very large values of ε′ and ε″ are because the charges build up at the interfaces between the polymer electrolyte and the electrodes [30, 40–43].

Moreover, addition of NH_4Cl into the FG matrix provides more H^+ ions suggesting larger mobile carriers. This presence of more mobile ions increases the interfacial polarisation and the larger will be the dielectric properties. This dielectric analysis shows higher dielectric constants for the highest conducting biopolymer electrolyte where more mobile charges are stored, and this is already confirmed by EIS analysis.

Modulus spectral analysis

The real part M_r and the imaginary part M_i of modulus are calculated using the equation

$$M_r = \frac{\varepsilon'}{\varepsilon'^2 + \varepsilon''^2} \tag{6}$$

$$M_i = \frac{\varepsilon''}{\varepsilon'^2 + \varepsilon''^2} \tag{7}$$

Figure 8(D, E) shows the variation in complex modulus in real and imaginary parts M_r and M_i as a function of frequency. Both real and imaginary moduli increase proportionally to the frequency [39]. At low frequencies, M_r and M_i approach zero (longer tail) which show negligible electrode polarisation. The extension of long tail exhibits longer relaxation time. The presence of peak at higher frequencies is due to the bulk effect of resistance. This behaviour confirms the non-Debye behaviour of the system. Though there is no definite peaks observed from modulus plots, the frequency dependant tan δ was plotted [44].

Tangent loss parameters is used to describe the dielectric relaxation process in SBEs. Dielectric loss is obtained by knowing the dielectric constant and dielectric loss from Eq. (8)

$$\tan\delta = \frac{\varepsilon_i}{\varepsilon_r} or \frac{M_i}{M_r} \tag{8}$$

Figure 8(C) gives the tan δ as a function of frequency. The curves reach maximum and thereafter it saturated at high frequency. This is because the number of charge carriers increases which decrease the resistivity. FG03 shows good electrical, dielectric property and ion transport in the presence of H^+ ions. The shift in the peaks towards higher frequency with increasing concentration above FG03 indicate more space charge polarisation due to rising number of grain boundaries. However, increasing NH_4Cl decreases the electrical performance and therefore the peak of FG04 shifted towards higher frequency.

Transport analysis

TNM measurement is used to determine the contribution of ions and electrons to the total conductivity [45]. These dominant charge species are responsible for conduction in the FG-NH_4Cl electrolyte system. Using Wagner's polarisation approach, the highest conducting electrolyte membrane FG03 is placed between two stainless steel blocking electrodes on applying 1.5-V DC voltage at ambient temperature. The current across the electrolyte as a function of time has been recorded. Figure 9 shows the polarisation current with respect to time plot of the highest conducting SPE. Knowing the initial and final currents, the transference number can be obtained from the equation as follows [5].

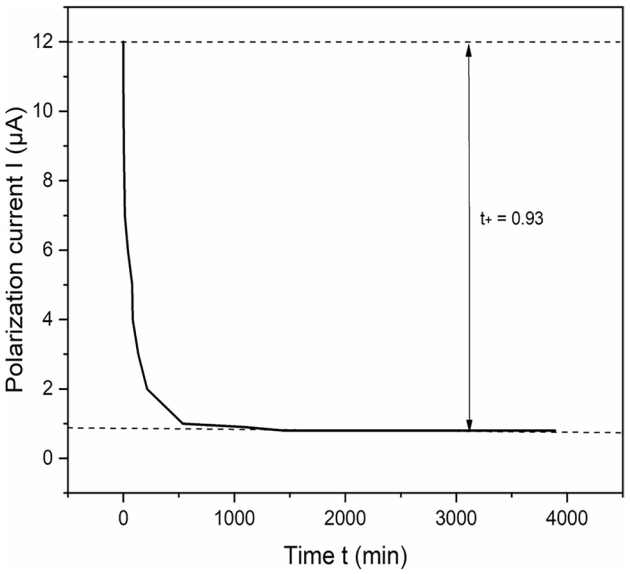

Fig. 9 Polarisation current Vs time plot for highest conducting polymer electrolyte FG03

$$t_+ = \frac{I_i - I_f}{I_i} \tag{9}$$

$$t_- = \frac{I_f}{I_i} \tag{10}$$

Here, t_+ is the transference number of cation, t_- is the transference number of anion, I_i represents the initial current at $t=0$ (due to both ions and electrons) and I_f is the current on saturation (due to electrons only). Therefore, from Fig. 9, $t_+ \sim 1$, which implies the highest conducting electrolyte, is purely ionic and can be predominantly due to H^+ proton. The current decreases gradually with time which is ascribed to complete the depletion of ionic charges.

The transient ionic current technique is followed to identify the number of conducting ions in the highest-conducting electrolyte [38]. The ionic mobility μ has been determined by the relation

$$\mu = \frac{d^2}{tv} \tag{11}$$

where d is the thickness of the film, t is the time of flight and v is the applied potential. The mobility of cation is determined using ionic mobility μ and transport number t_+ and the mobility of anion is determined by the difference between total ionic mobility and mobility of cation.

$$\mu_+ = \mu t_+ \tag{12}$$

$$\mu_- = \mu - \mu_+ \tag{13}$$

The diffusion coefficient of the polymer electrolyte is obtained by the following equation,

$$D = \frac{K_B T_a \sigma}{Ne^2} \tag{14}$$

where K_B is the Boltzman constant, T_a is the ambient temperature, σ is the ionic conductivity of the polymer electrolyte, N is the number of charge carriers and e is the charge of an electron. The diffusion coefficient of cation and anion is given by

$$D_+ = Dt_+ \tag{15}$$

$$D_- = D - D_+ \tag{16}$$

The calculated anionic and cationic mobilities and diffusion coefficient of cation and anion of the highest conducting polymer electrolyte are listed in Table 7. The conductivity of the optimal conducting polymer is caused by the high influence of mobility and diffusion coefficients.

Proton battery construction

A primary ammonium battery has been constructed using highly conducting polymer electrolyte. The cell parameters are listed in Table 8. The OCV is measured by connecting a multimeter parallel to the cell.

The possible reactions of anode and cathode are given as follows [33, 46]:

Table 8 Battery cell parameter

Cell parameters	Value
Area of the cell (cm^2)	1.327
Weight of anode (g)	0.3681
Weight of electrolyte (g)	0.12
Weight of cathode (g)	0.3266
Cell diameter (cm)	1.3
Cell thickness (mm)	1.27
OCV (V)	1.89 V
Current drawn (mA)	0.2

Table 7 Transport parameters of the highest conducting polymer

Highest conducting polymer	N (cm^{-3})	t_+	t_-	μ_+ (cm^2/VS)	μ_- (cm^2/VS)	D_+ (cm^2/S)	D_- (cm^2/S)
FG03	2.93×10^{24}	0.93	0.07	2.84×10^{-9}	0.22×10^{-9}	7.35×10^{-11}	0.55×10^{-11}

Anode reaction

$$nZn + ZnSO_4 \cdot 7H_2O \leftrightarrow Zn_{n+1}(SO_4) \cdot (7-2n)H_2O.2n(OH) + 2nH^+ + 2ne^-$$

$$Electrolyte: \ FG + 0.3 \ wt.\% \ of \ NH_4Cl \ film$$

Cathode reaction

$$PbO_2 + 4H^+ + 2e^- \leftrightarrow Pb^{2+} + 2H_2O$$
$$V_2O_5 + 6H^+ + 2e^- \leftrightarrow 2VO^{2+} + 3H_2O$$

Cell Configuration

$$Zn \ + \ ZnSO_4 \ \cdot 7H_2O \mid FG \ + \ 0.3 \ wt.\% \ of \ NH_4Cl \mid PbO_2 \ + \ V_2O_5 \ + \ electrolyte$$

The OCV of the fabricated battery with FG03 film as electrolyte was observed as 1.89 V at room temperature. The theoretical oxidation potential of Zn is − 0.7618, while the reduction potential of PbO_2 is 1.455 V and the difference between them gives the theoretical OCV to be ~ 2.2168 V. The measured OCV of the fabricated cell is low compared to the theoretical OCV [11]. The cell potential versus time plot is shown in Fig. 10. The region at which the voltage remains constant is the plateau region. It can be observed that the cell potential is high and stable for the first 3.5 h at 1.89 V. Later, the potential discharges and drops to 1.85 V beyond the plateau region.

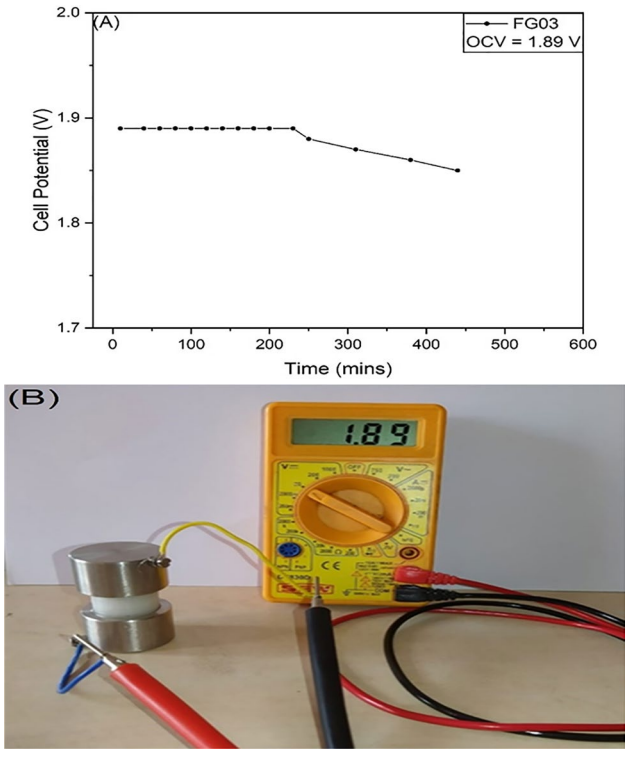

Fig. 10 Open-circuit voltage as a function of time for highest conducting polymer electrolyte FG03

A fixed load of 10 kΩ resistance is connected to the cell to study the discharge characteristics of the battery. The potential across the cell and the current through the constant load (10 kΩ) have been observed as a function of time (Fig. 11). The initial voltage is observed to be 1.89 V and it starts to decrease and remains constant at 1.23 V for about 2 days. Sikkanthar et al. have reported an OCV of 1.35 V with 75 PAN:25 NH_4Cl [36]. Selvalakshmi et al. have reported an OCV of 1.89 V [13]. Shreedatta Hegde reported PVA complexed with ammonium chloride exhibited an OCV of 0.567 V [38]. Hemalatha et al. have reported 75 Mwt% PVA:25 Mwt% proline:0.3 (m.m.%) of NH_4Cl polymer electrolyte with an OCV of 1.78 V [8]. The OCV exhibited in FG-NH_4Cl is high compared to other works.

Conclusion

The discovery of a new solid biopolymer electrolytes based on FG complexed with NH_4Cl were synthesised via solution casting technique. The reduction in the degree of crystallinity is confirmed by XRD pattern and the co-ordination of interactions between FG and NH_4Cl has been investigated by FTIR. The thermograms of DSC analysis show the lowest T_g of 52.34° for the highest conducting polymer electrolyte, which confirms the high segmental motion of the polymer chain. The EIS study reveals the enhancement of ionic conductivity by incorporation of NH_4Cl from 0.1 to 0.3 wt.%, and at 0.4 wt.%, the conductivity decreases by virtue of increasing ion clusters. The FG03 achieved a superior ionic conductivity of 1.13×10^{-4} S/cm at room temperature. The dielectric behaviour (frequency dependence of ε_r, M_r and tan δ) of the SBEs affirms the non-Debye behaviour at room

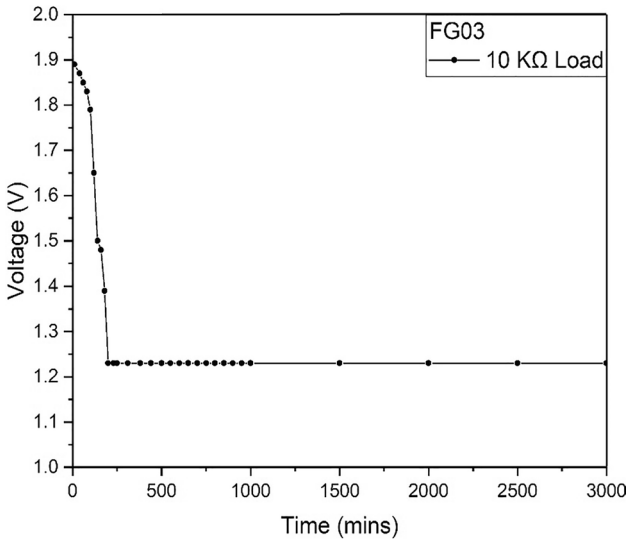

Fig. 11 Discharge curve of 10 K Ω load for highest conducting polymer electrolyte FG03

temperature. The transport of charge carriers has been examined using Wagner's polarisation technique, and it revealed that H^+ ions are the predominant conducting species in FG03 film. Thus the optimized conducting polymer FG03 has been applied for primary proton battery and it exhibited an OCV of 1.89 V. All these findings suggest that FG with NH_4Cl SBE perform as a potentially appealing membrane for proton batteries due to its high performance, economical affordability, environmental friendly and naturally abundant. Based on the performance of the prepared solid polymer electrolyte, the highest conducting polymer is a promising material for electrochemical applications.

Acknowledgements The authors would like to thank our college management for the help and support to carry out this work.

Data Availability The data presented in this study are available on request.

Declarations

Conflict of interest The authors declare no competing interests.

References

1. Sampath PVA, Subramanian S, Mathavan T, Benial AMF, Sindhuja M, Karthikeyan S (2016) Preparation and characterization of biopolymer electrolyte based on cellulose acetate for potential applications in energy storage devices. J Mat Sci: Materials in Electronics 27(9):9314–9324
2. Baskin I, Yair E-E (2022) Electrochemoinformatics as an emerging scientific field for designing materials and electrochemical energy storage and conversion devices—an application in battery science and technology. Adv Energy Mater 12(48):2202380
3. Diksha S, Sushant K, Abhimanyu S, Tejas S (2022) Ionic liquid–biopolymer electrolyte for electrochemical devices. Ionics 28:759–766
4. Kreuer K-D (2014) Ion conducting membranes for fuel cells and other electrochemical devices. Chem of Mater 26(1):361–380
5. Mehedi HM, Didarul Islam MD, Rashid TU (2020) Biopolymer-based electrolytes for dye-sensitized solar cells: a critical review. Energy Fuels 34(12):15634–15671
6. Johari SNAM, Nazrizawati AT, Hussein H, Siti KD (2021) A review: ionic conductivity of solid polymer electrolyte based polyethylene oxide. Int J Electrochem Sci 16(10):211049
7. Zubi G, Dufo-López R, Carvalho M, Pasaoglu G (2018) The lithium-ion battery: state of the art and future perspectives. Renew Sustain Energy Rev ISSN 89:1364–0321
8. Hemalatha R, Alagar M, Selvasekarapandian S, Sundaresan B, Moniha V, Boopathi G, Selvin PC (2019) Preparation and characterization of proton-conducting polymer electrolyte based on PVA, amino acid proline, and NH4Cl and its applications to electrochemical devices. Ionics 25(1):141–154
9. Brza MA, Aziz SB, Nofal MM, Saeed SR, Al-Zangana S, Karim WO, Kadir MF (2020) Drawbacks of low lattice energy ammonium salts for ion-conducting polymer electrolyte preparation structural morphological and electrical characteristics of CS PEO NH4BF4-based polymer blend electrolytes. Polymers 12(9):1885
10. Al Kiey SA, Hasanin MS, Heakal FET (2022) Green and sustainable chitosan–gum Arabic nanocomposites as efficient anticorrosive coatings for mild steel in saline media. Sci Rep 12(1):13209
11. Moniha V, Alagar M, Selvasekarapandian S, Sundaresan B, Hemalatha R, Boopathi G (2018) Synthesis and characterization of bio-polymer electrolyte based on iota-carrageenan with ammonium thiocyanate and its applications. J Solid State Electrochem 22(10):3209–3223
12. Shuhaimi NEA, Alias NA, Majid SR, Arof AK (2008) Electrical double layer capacitor with proton conducting κ-carrageenan chitosan electrolytes. Funct Mater Lett 1(3):195–201
13. Selvalakshmi S, Vanitha D, Saranya P, Selvasekarapandian S, Mathavan T, Premalatha M (2022) Structural and conductivity studies of ammonium chloride doped agar–agar biopolymer electrolytes for electrochemical devices. J Mater Sci: Mater Electron 33(32):24884–24894
14. Naachiyar RM, Ragam M, Selvasekarapandian S, Krishna MV, Buvaneshwari P (2021) Development of biopolymer electrolyte membrane using Gellan gum biopolymer incorporated with NH4SCN for electro-chemical application. Ionics 27(8):3415–3429
15. Periyajeyam B, Thangapandian M, Subramanian S, Manoharan VK, Ramadhasan MN, Ramasamy M (2022) Development and characterization of eco-friendly biopolymer gellan gum based electrolyte for electrochemical application. J Polym Eng 42(6):477–487
16. Monisha S, Mathavan T, Selvasekarapandian S, Benial AMF, Aristatil G, Mani N, Premalatha M (2017) Investigation of bio polymer electrolyte based on cellulose acetate-ammonium nitrate for potential use in electrochemical devices. Carbohyd Polym 157:38–47
17. Ma J, Sahai Y (2013) Chitosan biopolymer for fuel cell applications. Carbohyd Polym 92(2):955–975
18. Hai-Hua C, Yu-Sheng W, Yun L, Yang Z, Xia Z (2014) Effect of NaCl and sugar on physicochemical properties of flaxseed polysaccharide-potato starch complexes. Sci Asia 40:60
19. Rashid F, Ahmed Z, Hussain S, Huang JY, Ahmad A (2019) Linum usitatissimum L. seeds: flax gum extraction, physicochemical and functional characterization. Carbohyd Polym 215:29–38
20. Safdar B, Pang Z, Liu X, Jatoi MA, Mehmood A, Rashid MT, Naveed M (2019) Flaxseed gum: extraction, bioactive composition, structural characterization, and its potential antioxidant activity. J Food Biochem 43(11):e13014
21. Prado NS, Silva IS, Silva TA, Oliveira WJD, Motta LADC, Pasquini D, Otaguro H (2018) Nanocomposite films based on flaxseed gum and cellulose nanocrystals. Mater Res 21
22. Warrand J, Michaud P, Picton L, Muller G, Courtois B, Ralainirina R, Courtois J (2005) Structural investigations of the neutral polysaccharide of Linum usitatissimum L seeds mucilage. Int J Biol Macromolecules 35(3–4):121–125
23. Karami N, Kamkar A, Shahbazi Y, Misaghi A (2020) Effects of active chitosan-flaxseed mucilage-based films on the preservation of minced trout fillets: a comparison among aerobic, vacuum, and modified atmosphere packaging. Packag Technol Sci 33(11):469–484
24. Tee YB, Wong J, Tan MC, Talib RA (2016) Development of edible film from flaxseed mucilage. BioResources 11(4):10286–10295
25. Yu X, Huang S, Yang F, Qin X, Nie C, Deng Q, Geng F (2022) Effect of microwave exposure to flaxseed on the composition, structure and techno-functionality of gum polysaccharides. Food Hydrocoll 125:107447
26 Wang Y, Zhong WH (2015) Development of electrolytes towards achieving safe and high-performance energy-storage devices: a review. ChemElectroChem 2:22–36
27. Hadad S, Goli SAH (2018) Fabrication and characterization of electrospun nanofibers using flaxseed (Linum usitatissimum) mucilage. Int J Biol Macromol 114:408–414

28. Salleh NS, Aziz SB, Aspanut Z, Kadir MFZ (2016) Electrical impedance and conduction mechanism analysis of biopolymer electrolytes based on methyl cellulose doped with ammonium iodide. Ionics 22(11):2157–2167
29. Hodge RM, Edward GH, Simon GP (1996) Water absorption and states of ater in semicrystalline poly (vinyl alcohol) films. Polymer 37(8):1371–1376
30. Al Kiey SA, Hasanin MS (2021) Green and facile.synthesis of nickel oxide-porous carbon composite as improved electrochemical electrodes for supercapacitor application from banana peel waste. Environ Sci Pollut Res 28:66888–66900
31. Mazuki NF, Fuzlin AF, Saadiah MA, Samsudin AS (2019) An investigation on the abnormal trend of the conductivity properties of CMC/PVA-doped NH4Cl-based solid biopolymer electrolyte system. Ionics 25(6):2657–2667
32. Ishida H, Koenig JL (1978) Fourier transform infrared spectroscopic study of the structure of silane coupling agent on E-glass fiber. J Colloid Interface Sci 64(3):565–576
33. Monisha S, Selvasekarapandian S, Mathavan T, Milton Franklin Benial A, Manoharan S, Karthikeyan S (2016)Preparation and characterization of biopolymer electrolyte based on cellulose acetate for potential applications in energy storage devices. J Mater Sci: Mater Electron 27(9):9314–9324
34. Moni P (2021) Solid polymer electrolyte based on tragacanth gum-ammonium thiocyanate. J Solid State Electrochem 25(8):2371–2383
35. Chitra R, Vengadesh KM, Selvasekarapandian S (2022) Study on novel biopolymer electrolyte Moringa oleifera gum with ammonium nitrate. Polym Bull 79(6):3555–3572
36. Sikkanthar S, Karthikeyan S, Selvasekarapandian S, Arunkumar D, Nithya H, Junichi K (2016) Structural, electrical conductivity, and transport analysis of PAN–NH_4Cl polymer electrolyte system. Ionics 22(7):1085–1094
37. Jothi MA, Vanitha D, Bahadur SA, Nallamuthu N (2021) Investigations of biodegradable polymer blend electrolytes based on cornstarch: PVP: NH_4Cl and its potential application in solid-state batteries. J Mater Sci: Mater Electron 32:5427–5441
38. Hegde S, Ravindrachary V, Praveena SD, Guruswamy B, Sagar RN (2020) Microstructural, dielectric, and transport properties of proton-conducting solid polymer electrolyte for battery applications. Ionics 26(5):2379–2394
39. Fuzlin AF, Rasali NMJ, Samsudin AS (2018) Effect on ammonium bromide in dielectric behavior based Alginate Solid Biopolymer electrolytes. In IOP Conf Ser: Mater Sci Eng 342(1):012080
40. Hasanin M, Labeeb AM (2021) Dielectric properties of nicotinic acid/methyl cellulose composite via "green" method for anti-static charge applications. Mater Sci Eng, B 263:114797
41. Turky G, Moussa MA, Hasanin M, El-Sayed NS, Kamel S (2021) Carboxymethyl cellulose-based hydrogel: dielectric study, antimicrobial activity and biocompatibility. Arab J Sci Eng 46:17–30
42. Hasanin M, Mwafy EA, Youssef AM (2021) Electrical properties of conducting tertiary composite based on biopolymers and Polyaniline. J Bio-and Tribo-Corrosion 7(4):133
43. Al Kiey SA, Hasanin MS, Dacrory S (2021) Potential anticorrosive performance of green and sustainable inhibitor based on cellulose derivatives for carbon steel. J Mol Liq 338:116604
44. Majid SR, Arof AK (2007) Electrical behavior of proton-conducting chitosan-phosphoric acid-based electrolytes. Physica B 390(1–2):209–215
45. Yao P, Haobin Yu, Ding Z, Liu Y, Juan Lu, Lavorgna M, Junwei Wu, Liu X (2019) Review on polymer-based composite electrolytes for lithium batteries. Front Chem 7:522
46. Perumal P, Christopher SP, Selvasekarapandian S (2018) Characterization of biopolymer pectin with lithium chloride and its applications to electrochemical devices. Ionics 24(10):3259–3270